LANGMUIR

pubs.acs.org/Langmuir Article

# Modulating the Electronic Properties of Au−$MoS_2$ Interfaces Using Functionalized Self-Assembled Monolayers

Jenny K. Hedlund and Amy V. Walker*

Cite This: *Langmuir* 2020, 36, 682−688 Read Online

ACCESS | Metrics & More | Article Recommendations | Supporting Information

**ABSTRACT:** Molybdenum disulfide ($MoS_2$) is a transition-metal dichalcogenide with many applications including in electronic devices and sensors. A critical issue in the development of these devices is the high resistance between the metal contact and the molybdenum disulfide layer. In this study, we employ Raman spectroscopy and X-ray photoelectron spectroscopy to investigate the modification of Au−$MoS_2$ contact properties using functionalized alkanethiolate self-assembled monolayers (SAMs). We demonstrate that both 2H and 1T $MoS_2$ strongly interact with the underlying Au substrate. The electronic properties of the interface are mediated by the dipole moment of the alkanethiolate SAM, which have a $-CH_3$, $-CO_2C_6F_5$, −OH, or −COOH terminal group. Finally, we demonstrate the site-selective deposition of 2H and 1T $MoS_2$ on micropatterned SAMs to form conducting−semiconducting patterned $MoS_2$ films.

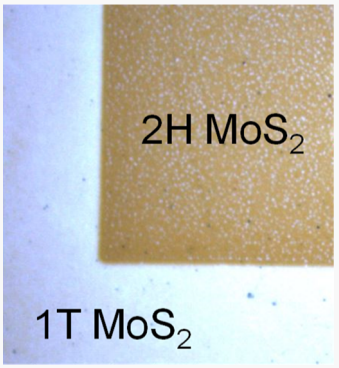




## INTRODUCTION

Molybdenum disulfide ($MoS_2$), a transition-metal dichalcogenide (TMD), has many applications including in energy storage, catalysis,[1] sensing,[2] and electronic devices.[3−6] These applications rely on the ability to tune the electronic properties of $MoS_2$. The thermodynamically stable form of $MoS_2$, 2H $MoS_2$, is a semiconductor. It has a unique transition from a direct band gap of ∼1.8 eV for monolayer $MoS_2$[7] to an indirect band gap of ∼1.2 eV for bulk $MoS_2$.[8] Additionally, metastable 1T $MoS_2$ can be synthesized, which is a semimetal.[9]

Although $MoS_2$ has many applications, a critical issue in the development of $MoS_2$ electronic devices and sensors is to lower the contact resistance between the metal electrodes and the $MoS_2$ layer.[3,4] For example, the performance of $MoS_2$ field effect transistors (FETs) strongly depends on the metal employed for the source and drain contacts.[3] Density functional theory (DFT) calculations show that the reason for this dependence is the significant valence and conduction band realignment of $MoS_2$ caused by the interface dipole formation between the metal electrode and the $MoS_2$ layer.[10−12] These studies also indicate that if the lattice parameter is altered, the magnitude of the $MoS_2$ band gap changes as well as switching from direct to indirect.[11,12] Further, after applying a tensile strain of ∼5% the band gap is reduced by ∼1 eV.[11]

In $MoS_2$ FETs, the most common electrode material is gold because the device characteristics are generally reasonable even though there is large energy offset between the gold electrode and $MoS_2$.[3,4,10] However, the contact resistance is very dependent on the deposition conditions of the gold contact, leading to large differences in device performance.[4] Experimental studies of gold layer and nanoparticle deposition on $MoS_2$ layers show that there are strong interactions between semiconducting 2H $MoS_2$ and the deposited gold.[7,13−15] In the Raman spectra, the $A_{1g}$ and $E^1_{2g}$ modes are red- and blue-shifted, respectively, indicating that the strain in the layer is between 1 and 3%, depending on the deposition.[13,14] Further, X-ray photoelectron spectra show that there is downward band bending at the $MoS_2$ surface, indicating that there is charge transfer between the gold and $MoS_2$ layers.[7] Mertens et al.[15] also demonstrated that the excitons in the $MoS_2$ monolayers couple with their mirror image in the Au substrate, indicating that the optical properties of $MoS_2$ are also strongly affected.

An alternative strategy is to use contact engineering to change the electronic properties of the $MoS_2$ and gold substrate. Here, we investigate using functionalized self-assembled monolayers (SAMs) to modify Au−$MoS_2$ contact properties. We employ chemical bath deposition (CBD) to deposit $MoS_2$ on SAMs at room temperature. It is noted that, although not performed here, the polycrystalline $MoS_2$ films can be laser annealed to form crystalline films for devices.[16] Functionalized SAMs modulate the work function of metal electrodes,[17−21] and have been demonstrated to improve the performance of organic devices such as thin-film transistors,[18,19] light-emitting diodes,[20] photodetectors,[20] and solar cells.[20,21] Using Raman spectroscopy and X-ray photoelectron

**Received:** June 26, 2019
**Revised:** December 23, 2019
**Published:** January 7, 2020




https://dx.doi.org/10.1021/acs.langmuir.9b01964
*Langmuir* 2020, 36, 682−688

spectroscopy (XPS), we demonstrate that both 2H and 1T $MoS_2$ strongly interact with the underlying Au substrate and alter the electronic properties of the $MoS_2$ layer. The interaction is mediated by the dipole moments of the alkanethiolate SAM, which have a $-CH_3$, $-CO_2C_6F_5$, $-OH$, or $-COOH$ terminal group. We also note that the surface energy of the functionalized SAM also determined whether 1T or 2H $MoS_2$ is deposited.[22] Semiconducting 2H $MoS_2$ films are deposited on $-CH_3$- and $-CO_2C_6F_5$-terminated SAMs, while 1T $MoS_2$ films are deposited on $-OH$- and $-COOH$-terminated SAMs. The formation of patterned multifunctional SAMs are relatively facile.[23,24] We, therefore, demonstrate the site-selective deposition of 2H and 1T $MoS_2$ on micropatterned SAMs to form conducting−semiconducting patterned $MoS_2$ films.

## EXPERIMENTAL SECTION

**Materials.** Hexadecanethiol (99+%), 16-mercaptohexadecanoic acid (90+%), 16-hydroxy-1-hexadecanethiol (99+%), and ammonium molybdate (99.98%) were purchased from Sigma-Aldrich (St. Louis, MO). Hydrazine hydrate (98+%), pentafluorophenol (PFP) (99%), 1-(3-dimethylaminopropyl)-3-ethylcarbodiimide hydrochloride (EDC) (98+%), and thioacetamide (99% ACS grade) were obtained from Alfa Aesar, Inc. (Ward Hill, MA). Finally, 14 .8 M ammonium hydroxide was acquired from Ward's Science+ (Rochester, NY). All reactants were used as received without any further purification.

**Preparation of SAMs.** The preparation of $-OH$-, $-COOH$-, and $-CH_3$-terminated alkanethiolate SAMs on Au used in this study is described in refs 25 and 26. Gold substrates were prepared by sequentially thermally depositing ∼200 Å Cr followed by ∼1000 Å Au on Si wafers (⟨111⟩ orientation; Addison Engineering Inc., San Jose, CA). A well-ordered SAM is prepared by immersing a gold substrate into a 1 mM ethanolic solution of alkanethiol (with the $-OH$, $-COOH$, or $-CH_3$ terminal group) in ethanol for 24 h at ambient temperature.

Perfluorinated SAMs ($-CO_2C_6F_5$-terminated SAMs) on Au were prepared using the method described in ref 27. A $-COOH$-terminated SAM was immersed into 0.1 M EDC and 0.2 M PFP isopropanolic solution for 5 h. The substrate was then thoroughly rinsed with deionized water and ethanol, and dried using nitrogen gas.

To ensure that the functionalized SAMs were free from chemical contamination, the samples were characterized using single-wavelength ellipsometry, time-of-flight secondary ion mass spectrometry, and XPS.

**UV Photopatterning of SAMs.** The $-OH$- and $-COOH$-terminated SAMs were photopatterned using the procedures described by Zhou and Walker.[23] Briefly, a mask (copper TEM grid; Electron Microscopy Inc., Hatfield PA) was positioned on top of a $-OH$- or $-COOH$-terminated SAM. The construct was then placed ∼50 mm from a 500 W Hg arc lamp with a narrow band-pass UV filter (280 to 400 nm) and a dichroic mirror (Thermal Oriel—Spectra Physics Inc., Stratford CT). The sample was then exposed to UV light for 2 h. The photopatterned SAM was then rinsed with ethanol and immersed in a 1 mM ethanolic solution of the $-CH_3$-terminated SAM for 24 h at room temperature. In the areas exposed to UV light, the photooxidized SAM was displaced by the $-CH_3$-terminated SAM, creating a multifunctional patterned $-COOH/-CH_3$ or $-OH/-CH_3$ SAM. The samples were then washed with ethanol, dried with $N_2$ gas, and used immediately.

**CBD of $MoS_2$.** CBD of $MoS_2$ was carried out using the method described by Hedlund and Walker.[22] Briefly, to 10 mL of aqueous solution containing 5% ammonium molybdate, 15 mL of 14.8 M ammonium hydroxide and then 10 mL of 80% hydrazine hydrate were added while continuously stirring. To form the $MoS_2$ deposition bath, 15 mL of 1 M thioacetamide was then added. Depositions were performed for 24 h at room temperature, 21 ± 2 °C. After deposition, the samples were rinsed with deionized water and dried with nitrogen gas prior to XPS or Raman spectroscopic analyses.

**Raman Spectroscopy and Mapping.** Raman spectra were obtained using a Thermo Scientific DXR Raman microscope (Thermo Scientific, Madison WI) equipped with a 50× objective lens and 25 $\mu$m slit aperture. The laser wavelength was 532 nm. Raman spectra were collected with laser powers of 1.0 mW. To generate Raman maps, spectra were collected at 10 $\mu$m intervals in the defined image area using 0.3 mW laser power. Images were obtained on a "heat scale" from these spectra at selected frequencies.

In order to reduce interference from fluorescence, "fluorescence correction" was used and the samples photobleached for 30 s prior to data collection.

Optical images of the samples were also obtained using the integrated microscope.

The spectra and images shown are representative of the data collected using multiple samples (at least three samples per experimental condition).

**X-ray Photoelectron Spectroscopy.** Ex situ X-ray photoelectron spectra were acquired using a PHI VersaProbe II Scanning XPS Microprobe (Physical Electronics Inc., Chanhassen MN). High-resolution spectra were collected using a monochromatic Al K$\alpha$ X-ray source ($E_p$ = 1486.7 eV), pass energy of 23.5 eV, energy step of 0.2 eV, and analysis angle of 45°. All photoelectron spectra were obtained using a charge compensation system which employs both electron and ion beams. The binding energies were calibrated to the Au $4f_{7/2}$ (84.0 eV) binding energies. Spectra were analyzed using CasaXPS 2.3.17 (RBD Instruments, Inc., Bend, OR). All spectra shown are representative of the data collected.

## RESULTS AND DISCUSSION

**Effect of the Au Substrate on $MoS_2$ Deposition.** After deposition on the functionalized SAMs, the Raman data show that the functionalized SAM substrate strongly affects the spectra of the deposited $MoS_2$ layer (Figure 1). For 1T and 2H

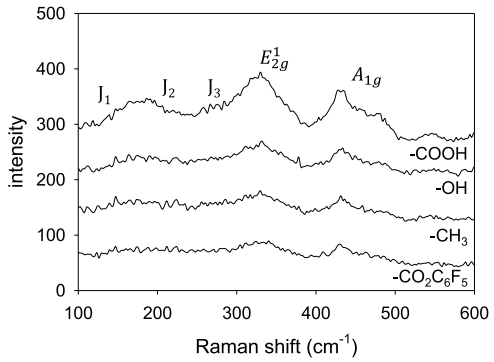


**Figure 1.** Raman spectra of $MoS_2$ films deposited on $-COOH$-, $-OH$-, $-CH_3$-, and $-CO_2C_6F_5$-terminated SAMs. Deposition time: 24 h.

$MoS_2$, it is well known that there are two principal Raman-active modes, $E^1_{2g}$ (∼383 $cm^{-1}$) and the $A_{1g}$ (∼408 $cm^{-1}$).[28,29] For 1T $MoS_2$, there are three additional Raman-active modes, $J_1$ (∼160 $cm^{-1}$), $J_2$ (225 $cm^{-1}$), and $J_3$ (∼335 $cm^{-1}$).[29] In Figure 1, it can be clearly seen that on $-CH_3$- and $-CO_2C_6F_5$-terminated SAMs, there is also a very weak broad mode at ∼185 $cm^{-1}$, which we attribute to the red-shifted ($A_{1g}$ − LA(M)) mode. For $-COOH$- and $-OH$-terminated SAMs in Figure 1, there is an additional broad peak at ∼170 $cm^{-1}$, which suggests the presence of the $J_1$ and $J_2$ modes of 1T $MoS_2$. We also observe that the $E^1_{2g}$ mode has a larger FWHM (∼30 $cm^{-1}$) than the corresponding $E^1_{2g}$ mode on $-CH_3$- and $-CO_2C_6F_5$-terminated SAMs (∼25 $cm^{-1}$), which suggests that the $E^1_{2g}$ mode is convolved with the $J_3$ 1T $MoS_2$ mode. As the deposited $MoS_2$ layer becomes thicker (longer deposition


https://dx.doi.org/10.1021/acs.langmuir.9b01964
Langmuir 2020, 36, 682−688

time), the $E^1_{2g}$ and the $A_{1g}$ modes become narrower and have peak positions at 382 and 405 $cm^{-1}$, respectively (Figure 2). On −COOH- and −OH-terminated SAMs the $J_1$, $J_2$, and $J_3$ become separate, narrower peaks confirming that 1T $MoS_2$ has deposited (Figure 2).

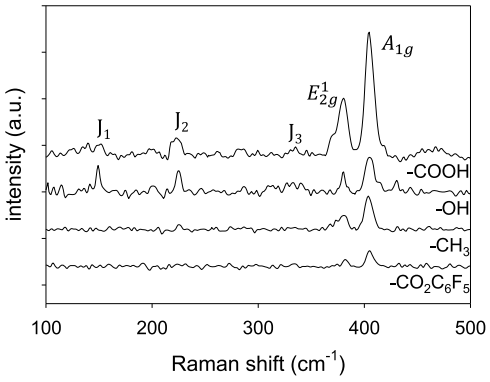


**Figure 2.** Raman spectra of thicker $MoS_2$ films deposited on −COOH-, −OH-, $-CH_3$-, and $-CO_2C_6F_5$-terminated SAMs. Deposition was performed for 48 h.

We note that similar effects have been observed in Raman spectra after deposition of gold thin films or nanoparticles on 2H $MoS_2$.[13,14] However, the red- and blue-shifts of the out-of-plane $A_{1g}$ and in-plane $E^1_{2g}$ modes, respectively, tend to be smaller (less than 15 $cm^{-1}$). The red and blue shifts of the $A_{1g}$ and $E^1_{2g}$ modes can be attributed to the following effects.[13] The $A_{1g}$ mode is due to the symmetric vibration of S atoms along the *c*-axis (vertical axis) of $MoS_2$. The interaction between the deposited gold and $MoS_2$ stiffens this vibration, leading to a blue shift of the phonon mode. The in-plane $E^1_{2g}$ mode is due to the lattice vibration of the Mo and S atoms in opposite directions. The deposited gold has a large dielectric constant which increases the screening of electron−electron interactions in the $MoS_2$, which weakens the planar interionic interactions. This effect leads to a red shift of the $E^1_{2g}$ mode. In addition, a broadening of the $E^1_{2g}$ mode is observed, which is attributed to the inhomogeneous contact between the Au and $MoS_2$ layers. Gong and co-workers[13] describe the Au−$MoS_2$ contact as one in which there are some areas in which Au and $MoS_2$ are in intimate contact, while there are some regions where the metal is at a large distance above the $MoS_2$ surface. These observations suggest that the interaction of the deposited $MoS_2$ with the underlying gold substrate, and not the SAM, is the dominant effect in the Raman spectra. The red shift in the $E^1_{2g}$ mode also indicates that there is a larger induced biaxial strain in the $MoS_2$ than for gold deposited on $MoS_2$. Using the experimentally derived and theoretically supported "4.5 $cm^{-1}$/%" rule,[13,14] we estimate that the strain in the $MoS_2$ layer is ∼11.8%, which is very large! Such strain is unlikely to be accommodated by the $MoS_2$ layer, indicating that there are areas in intimate contact with the underlying functionalized SAM substrate and areas in which the film is not in intimate contact, which is consistent with the broad modes observed in the Raman spectra (Figure 1).

On −OH- and −COOH-terminated SAMs, 1T $MoS_2$ is deposited and the $J_1$, $J_2$, and $J_3$ modes are also broadened but there are smaller apparent peak shifts than the $E^1_{2g}$ and $A_{1g}$ modes (Figure 1). The $J_1$, $J_2$, and ($A_{1g}$ − LA(M)) modes appear convolved together, whereas the $J_3$ mode is combined with the $E^1_{2g}$ mode (Figure 1). The $J_1$ mode involves two different types of vibrations:[30] an out-of-plane motion of the Mo atoms and will be red-shifted, and an in-plane shearing vibration of the Mo and S atoms and will be blue-shifted. Thus, the peak position is unlikely to significantly shift because of these opposite effects. Similarly, the $J_2$ and $J_3$ modes involve both in-plane and out-of-plane motions of $MoS_2$,[30] and so will not be significantly shifted in position. We also attribute the mode broadening to the inhomogeneous contact between the Au substrate and $MoS_2$.[13]

X-ray photoelectron spectra studies of the deposited $MoS_2$ provide an estimate of the film thickness. Using the uniform layer model, after 24 h of deposition, the films are ∼4.0 nm thick (∼6 layers).[22] Further, the XPS data are in agreement with the Raman spectra and confirm that the film interacts with the underlying gold substrate. Figure 3 displays the Mo 3d and

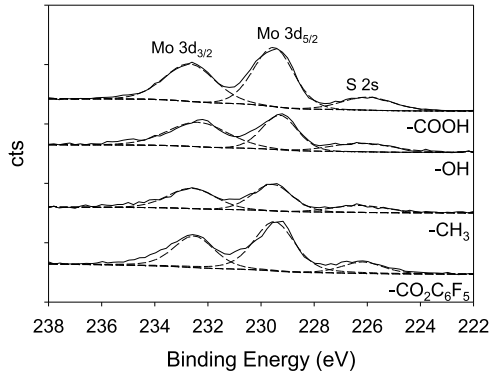


**Figure 3.** Mo 3d and S 2s photoelectron spectra of $MoS_2$ films deposited on −COOH-, −OH-, $-CH_3$-, and $-CO_2C_6F_5$-terminated SAMs. Deposition time: 24 h.

S 2s photoelectron spectra of the deposited $MoS_2$ film on the functionalized alkanethiolate SAMs on gold. Three peaks are observed at ∼232.5, ∼229.4, and ∼226.3 eV, which are assigned to the Mo $3d_{3/2}$, Mo $3d_{5/2}$, and S 2s peaks of $MoS_2$, and suggest that 2H $MoS_2$ has deposited on all SAM substrates.[31] However, upon exfoliation[32] for $MoS_2$ deposited on −COOH- and −OH-terminated SAMs, the Mo 3d and S 2s photoelectron peaks have lower binding energies by ∼0.9 eV, clearly indicating that 1T $MoS_2$ has deposited and this assignment is confirmed by Raman spectra of the exfoliated $MoS_2$ films.[22] The surprising binding energies of 1T $MoS_2$ on −OH- and −COOH-terminated SAMs can be caused by a number of reasons such as surface charging during data acquisition, changes in the film stoichiometry, and the interaction of the $MoS_2$ film with the SAM substrate. During data acquisition, photoelectrons are generated and so it is likely that the $MoS_2$ film will charge positively, leading to changes in binding energy. However, this is unlikely because charge compensation was employed, and no change in binding energy was observed for 2H $MoS_2$ films deposited on $-CH_3$ and $-CO_2C_6F_5$ SAMs, which were measured using the same experimental parameters. Further, the C 1s and O 1s energies do not change their binding energies; these are expected if there is surface charging. Additionally, the calculated S/Mo ratios are equal to 2.0 with experimental error, indicating that the deposited films are stoichiometric $MoS_2$ on all substrates studied (see Supporting Information Table S1). Rather, the binding energies of the Mo 3d, S 2s, and 2p states suggest that there is an interaction between the substrate and the deposited


https://dx.doi.org/10.1021/acs.langmuir.9b01964
Langmuir 2020, 36, 682−688

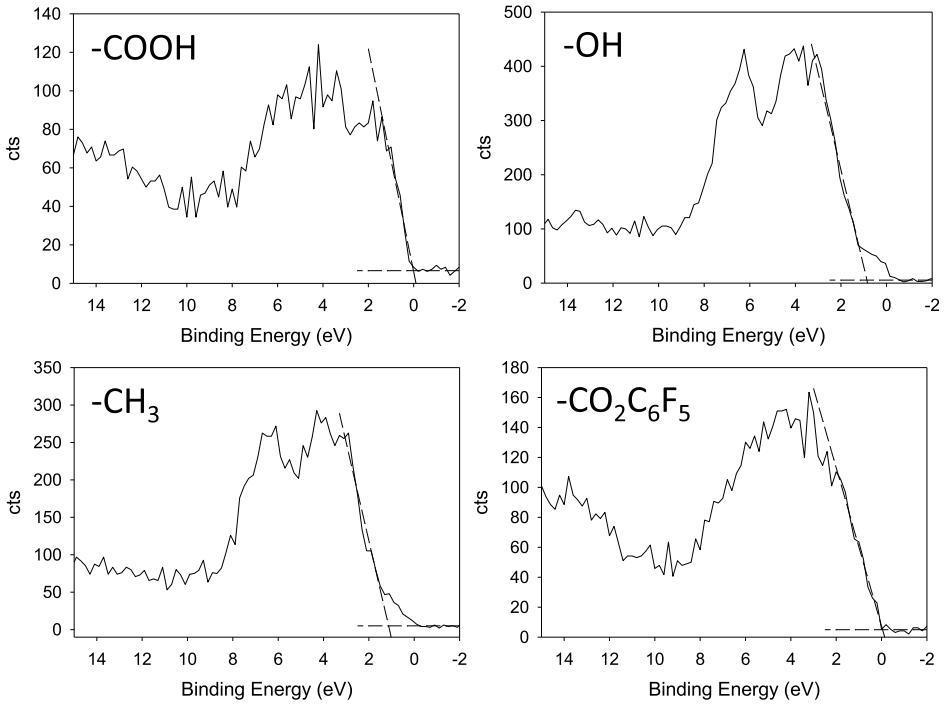


**Figure 4.** Valence band photoelectron spectra of $MoS_2$ films deposited on −COOH-, −OH-, $-CH_3$-, and $-CO_2C_6F_5$-terminated SAMs. Deposition time: 24 h.

$MoS_2$ layer. We also note that the photoelectron peak intensities are ≳4× those observed on the exfoliated films for similar film thicknesses, which suggests that there is charge transfer between the substrate and the deposited film. Similar effects have been observed by Jiang et al.[33] for the Au clusters deposited on rutile $TiO_2$(110).

Taken together, the Raman scattering and XPS data suggest that the underlying gold substrate interacts with the deposited $MoS_2$ layer. DFT calculations show that there is significant valence and conduction band realignment of $MoS_2$ caused by the interface dipole formation between a metal electrode and the $MoS_2$ layer.[10,11] Further, these studies reveal that these effects were dependent on the distance between the metal electrode and $MoS_2$ layer.[10] However, we note that the offsets rapidly decrease with the metal−$MoS_2$ distance and for Au are close to zero by ∼5 Å, which is much shorter than the SAM film thickness (∼20 Å). Thus, the interaction between the Au substrate and deposited $MoS_2$ is likely due to charge transfer mediated by the net dipole moment of the SAMs. There are two contributions to the dipole moment of the alkanethiolate SAM: the bond dipole because of the Au−S interface and the dipole moments of the molecules within the SAM.[19,34] The orientation and magnitude of this SAM dipole is therefore dependent on the chemical composition of the SAM, including its alkyl chain length and functional groups,[19,34,35] and has been demonstrated to increase and decrease the work function of gold.[21,34,36] Further, the surface dipole moments of functionalized SAMs have been employed to control the charge channel density of organic thin-film transistors[18] as well as the properties of superhydrophobic surfaces.[34,37]

To investigate the effect of the SAM substrate adsorbed on gold on the $MoS_2$ deposit, we obtained valence band (VB) XPS data. Figure 4 displays the VB spectra of the deposited $MoS_2$ film on the functionalized alkanethiolate SAMs on gold. On −COOH-terminated SAMs, there is photoelectron intensity from the Mo 4d band (VB) at a binding energy of 0 eV, which is the Fermi level of the system, and indicates that the $MoS_2$ layer is metallic 1T $MoS_2$. We also note that after exfoliation from the −COOH-terminated SAM substrate, the valence band maximum (VBM) is also observed at 0 eV.[22] On −OH-terminated SAMs, the VBM is 0.8 eV, which is the same as the exfoliated $MoS_2$ film (0.7 eV)[22] (within experimental error) and is consistent with the deposition of semimetallic 1T $MoS_2$. Since the Raman modes are shifted and there is an increase in the Mo- and S- energies, we suggest that there is charge transfer between the substrate and deposited $MoS_2$ to level their Fermi energies. For semiconducting 2H $MoS_2$ films deposited on $-CH_3$- and $-CO_2C_6F_5$-terminated SAMs, the interaction of the underlying gold substrate with the film will lead to surface band bending. After $MoS_2$ deposition on the $-CH_3$-terminated SAMs and mechanical exfoliation, the VBM is at 1.3 eV, which is consistent with the band gap of multilayer $MoS_2$.[22] For the $MoS_2$ film on the $-CH_3$-terminated SAM, the VBM is reduced by 0.3 to 1.0 eV, which we attribute to surface band bending because of charge transfer between the Au substrate and the deposited $MoS_2$. For the $-CO_2C_6F_5$-terminated SAMs, the reduction in the VBM is much larger; the VBM is reduced from 1.0 eV for the exfoliated $MoS_2$ film[22] to 0.0 eV for the unexfoliated $MoS_2$ film (i.e., on the $-CO_2C_6F_5$-terminated SAM substrate), indicating that there is a larger transfer between the Au substrate and the $MoS_2$ film.[34,35] Finally, we note that for $MoS_2$ films deposited on −OH- and $-CH_3$-terminated SAMs, there is also a small tail in front of the VB edge, which likely arises from gap-induced surface states.

The changes in the VBM maxima for $MoS_2$ deposited on the −OH-, $-CH_3$-, and $-CO_2C_6F_5$-terminated SAMs are likely because of three effects. First, the energy alignment of the functionalized SAM-gold electrode with the $MoS_2$ will be different for 1T and 2H $MoS_2$. Second, there is likely strain in


https://dx.doi.org/10.1021/acs.langmuir.9b01964
Langmuir 2020, 36, 682−688

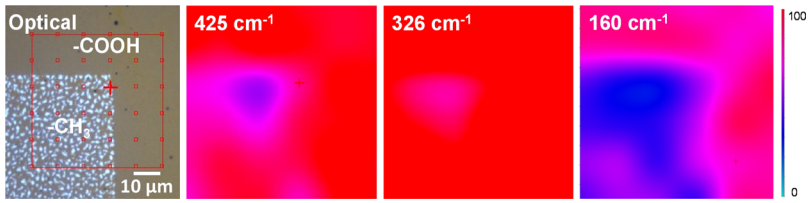


**Figure 5.** Optical and Raman spectroscopic images at 425, 326, and 160 $cm^{-1}$ of $MoS_2$ films deposited on a patterned $-COOH/-CH_3$-terminated SAM. Deposition time: 24 h. The Raman spectroscopic images are shown on a heat scale, and the area and points of analysis are shown in red on the optical image.

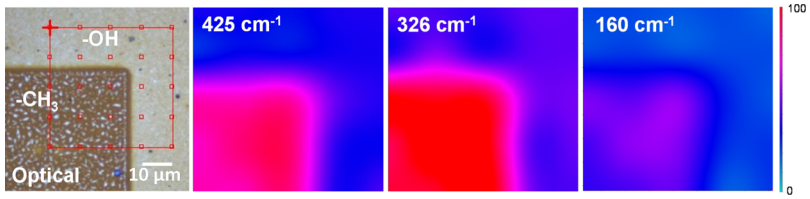


**Figure 6.** Optical and Raman spectroscopic images at 425, 326, and 160 $cm^{-1}$ of $MoS_2$ films deposited on a patterned $-OH/-CH_3$-terminated SAM. Deposition time: 24 h. The Raman spectroscopic images are shown on a heat scale, and the area and points of analysis are shown in red on the optical image.

the $MoS_2$ layer, which is induced by the lattice mismatch between the SAM and $MoS_2$. Third, the dipole moment of the SAM affects the work function of the Au substrate, which in turn affects the $MoS_2$ band alignment. For the $-CH_3$-terminated SAMs, the work function of the Au substrate increases, whereas for the perfluorinated SAM, the gold work function decreases. The large change in the VBM for $MoS_2$ on the $-CO_2C_6F_5$-terminated SAMs can be attributed to better energy alignment between the gold electrode and the deposited $MoS_2$ layer.

**Site-Selective Deposition of $MoS_2$ Polytypes.** These results indicate that by manipulating the surface chemistry, the $MoS_2$ CBD can be used to selectively deposit different $MoS_2$ polytypes and modulate the film conductivity in a spatially resolved way. Thus, $MoS_2$ CBD has the potential to create self-aligned device structures where both the $MoS_2$ polytype and band gap can be modulated. To demonstrate this process, we employ micropatterned functionalized SAMs to form two structures. First, a patterned $-COOH/-CH_3$-terminated SAM substrate a 1T/2H $MoS_2$ deposit is synthesized with areas which are conductive and semiconducting, respectively. Second, using a patterned $-OH/-CH_3$-terminated SAM substrate, a 1T/2H $MoS_2$ patterned film is deposited with two different band gaps.

Figure 5 displays an optical image of the $MoS_2$ film deposited on a patterned $-COOH/-CH_3$-terminated SAM and images of the Raman mode intensities at 425, 326, and 160 $cm^{-1}$. In the optical image, it can be seen that the $MoS_2$ film deposited on the $-CH_3$-terminated SAM appears to be thicker and rougher than on the $-COOH$-terminated SAM. The Raman spectra also indicate that there is some disorder present in the deposited $MoS_2$ film (see Supporting Information Figure S2). The mode intensities at 425 and 326 $cm^{-1}$, which are characteristic of the $A_{1g}$ and $E^1_{2g}$ modes, are similar in the $-CH_3$- and $-COOH$-terminated SAM areas (Figure 5). In contrast, at 160 $cm^{-1}$, which is characteristic of the $J_1$ mode, the relative intensity is larger in the $-COOH$-terminated SAM area, indicating that 1T $MoS_2$ has deposited. The peak is 76 ± 5% of the $A_{1g}$ mode intensity, which is larger than for the $-CH_3$-terminated SAM (61 ± 4%).

For $MoS_2$ deposited on a patterned $-OH/-CH_3$-terminated SAM, in the optical image, it can be clearly seen that the $MoS_2$ film deposited on the $-CH_3$-terminated SAM appears to be thicker, similar to the patterned $-OH/-CH_3$-terminated SAM (Figure 6). The spectra of the $MoS_2$ layer from the $-CH_3$-terminated SAM area are more intense, which is consistent with the difference in the film thicknesses on the $-OH$- and $-CH_3$-terminated SAMs (see Supporting Information Figure S2). In the Raman images, the mode intensities at 425 and 326 $cm^{-1}$, which are characteristic of the $A_{1g}$ and $E^1_{2g}$ modes are therefore stronger in the $-CH_3$-terminated SAM areas (Figure 6). In contrast, the images at 160 $cm^{-1}$ show a uniform Raman intensity, which is consistent with the presence of $J_1$ mode, indicating that 1T $MoS_2$ has deposited on the $-OH$-terminated SAM.

## ■ CONCLUSIONS

In summary, both 1T and 2H $MoS_2$ strongly interact with the underlying gold substrate, which is mediated by the dipole moment of the functionalized SAM. Using VB XPS, we show that for 1T $MoS_2$ deposited on $-COOH$-terminated SAMs, the VBM remains at 0 eV, indicating that the layer is metallic and the Fermi levels of the gold and $MoS_2$ are aligned. For 1T $MoS_2$ deposited on $-OH$-terminated SAMs, the VBM is reduced by 0.2 eV, indicating that there is charge transfer between the Au and $MoS_2$. For semiconducting 2H $MoS_2$ films deposited on $-CH_3$ and $-CO_2C_6F_5$-terminated SAMs, the interaction of the underlying gold substrate with the film leads to surface band-bending. On $-CH_3$-terminated SAM, the VBM is significantly reduced from 1.3 eV for the exfoliated $MoS_2$ film to 0.8 eV. For $-CO_2C_6F_5$-terminated SAMs, the reduction in the VBM is much larger from 1.0 eV for the exfoliated $MoS_2$ film to 0.0 eV. We attribute the larger reduction in the VBM to an increase in charge transfer between the Au substrate and the $MoS_2$ film mediated by the larger dipole of perfluorinated SAMs.

We have also demonstrated the area-selective deposition of 2H and 1T $MoS_2$ on micropatterned SAMs. A patterned $-COOH/-CH_3$-terminated SAM substrate, a patterned 1T, and 2H $MoS_2$ deposit are synthesized with areas which are


https://dx.doi.org/10.1021/acs.langmuir.9b01964
Langmuir 2020, 36, 682−688

conductive and semiconducting, respectively. A patterned 1T and 2H $MoS_2$ film with two different band gaps is deposited using a patterned $-OH/-CH_3$-terminated SAM substrate. This work therefore presents a surface-templated method for the synthesis of $MoS_2$ layers with a controlled polytype and shows that the electronic properties can be modulated by choice of substrate.

## ■ ASSOCIATED CONTENT

### Supporting Information

The Supporting Information is available free of charge at https://pubs.acs.org/doi/10.1021/acs.langmuir.9b01964.

Ratio of S to Mo determined by XPS for $MoS_2$ films deposited on $-COOH$-, $-OH$-, $-CH_3$-, and $-CO_2C_6F_5$-terminated SAMs; Raman spectra of $MoS_2$ films from $-OH$- and $-CH_3$-terminated SAM areas after deposition on a patterned $-COOH/-CH_3$-terminated SAM; Raman spectra of $MoS_2$ films from $-OH$- and $-CH_3$-terminated SAM areas after deposition on a patterned $-OH/-CH_3$-terminated SAM (PDF)

## ■ AUTHOR INFORMATION


### Corresponding Author

**Amy V. Walker** − *University of Texas at Dallas, Richardson, Texas;* orcid.org/0000-0003-2114-3644; Phone: +1 972 883 5780; Email: amy.walker@utdallas.edu; Fax: +1 972 883 5725

### Other Author

**Jenny K. Hedlund** − *University of Texas at Dallas, Richardson, Texas;* orcid.org/0000-0001-8569-802X

Complete contact information is available at: https://pubs.acs.org/10.1021/acs.langmuir.9b01964


### Author Contributions

The manuscript was written through contributions of all authors.


### Funding

National Science Foundation CHE 1708259.


### Notes

The authors declare no competing financial interest.


## ■ ACKNOWLEDGMENTS

The authors gratefully acknowledge support from the National Science Foundation (CHE 1708258) and Dr. K. J. Cho for many useful discussions.


## ■ ABBREVIATIONS

TMD, transition-metal dichalcogenide; FET, field effect transistor; DFT, density functional theory; XPS, X-ray photoelectron spectroscopy; SAM, self-assembled monolayer; PFP, pentafluorophenol; EDC, 1-(3-dimethylaminopropyl)-3-ethylcarbodiimide; TEM, transmission electron microscopy

## ■ REFERENCES


(1) Li, M.; Wang, D.; Li, J.; Pan, Z.; Ma, H.; Jiang, Y.; Tian, Z. Facile hydrothermal synthesis of $MoS_2$ nano-sheets with controllable structures and enhanced catalytic performance for anthracene hydrogenation. *RSC Adv.* **2016**, *6*, 71534−71542.

(2) Lopez-Sanchez, O.; Lembke, D.; Kayci, M.; Radenovic, A.; Kis, A. Ultrasensitive photodetectors based on monolayer $MoS_2$. *Nat. Nanotechnol.* **2013**, *8*, 497.

(3) Kappera, R.; Voiry, D.; Yalcin, S. E.; Branch, B.; Gupta, G.; Mohite, A. D.; Chhowalla, M. Phase-engineered low-resistance contacts for ultrathin $MoS_2$ transistors. *Nat. Mater.* **2014**, *13*, 1128.

(4) English, C. D.; Shine, G.; Dorgan, V. E.; Saraswat, K. C.; Pop, E. Improved Contacts to $MoS_2$ Transistors by Ultra-High Vacuum Metal Deposition. *Nano Lett.* **2016**, *16*, 3824−3830.

(5) Radisavljevic, B.; Radenovic, A.; Brivio, J.; Giacometti, V.; Kis, A. Single-layer $MoS_2$ transistors. *Nat. Nanotechnol.* **2011**, *6*, 147−150.

(6) Wang, Q. H.; Kalantar-Zadeh, K.; Kis, A.; Coleman, J. N.; Strano, M. S. Electronics and optoelectronics of two-dimensional transition metal dichalcogenides. *Nat. Nanotechnol.* **2012**, *7*, 699.

(7) Lin, Y.-K.; Chen, R.-S.; Chou, T.-C.; Lee, Y.-H.; Chen, Y.-F.; Chen, K.-H.; Chen, L.-C. Thickness-Dependent Binding Energy Shift in Few-Layer $MoS_2$ Grown by Chemical Vapor Deposition. *ACS Appl. Mater. Interfaces* **2016**, *8*, 22637−22646.

(8) Benavente, E.; Santa Ana, M. A.; Mendizábal, F.; González, G. Intercalation chemistry of molybdenum disulfide. *Coord. Chem. Rev.* **2002**, *224*, 87−109.

(9) Wypych, F.; Schöllhorn, R. 1T-MoS2, a new metallic modification of molybdenum disulfide. *J. Chem. Soc., Chem. Commun.* **1992**, 1386−1388.

(10) Gong, C.; Colombo, L.; Wallace, R. M.; Cho, K. The Unusual Mechanism of Partial Fermi Level Pinning at Metal−$MoS_2$ Interfaces. *Nano Lett.* **2014**, *14*, 1714−1720.

(11) Farmanbar, M.; Brocks, G. First-principles study of van der Waals interactions and lattice mismatch at $MoS_2$/metal interfaces. *Phys. Rev. B* **2016**, *93*, 085304.

(12) Bruix, A.; Miwa, J. A.; Hauptmann, N.; Wegner, D.; Ulstrup, S.; Grønborg, S. S.; Sanders, C. E.; Dendzik, M.; Grubišić Čabo, A.; Bianchi, M.; Lauritsen, J. V.; Khajetoorians, A. A.; Hammer, B.; Hofmann, P. Single-layer $MoS_2$ on Au(111): Band gap renormalization and substrate interaction. *Phys. Rev. B* **2016**, *93*, 165422.

(13) Gong, C.; Huang, C.; Miller, J.; Cheng, L.; Hao, Y.; Cobden, D.; Kim, J.; Ruoff, R. S.; Wallace, R. M.; Cho, K.; Xu, X.; Chabal, Y. J. Metal Contacts on Physical Vapor Deposited Monolayer $MoS_2$. *ACS Nano* **2013**, *7*, 11350−11357.

(14) Gołasa, K.; Grzeszczyk, M.; Binder, J.; Bożek, R.; Wysmołek, A.; Babiński, A. The disorder-induced Raman scattering in Au/$MoS_2$ heterostructures. *AIP Adv.* **2015**, *5*, 077120.

(15) Mertens, J.; Shi, Y.; Molina-Sánchez, A.; Wirtz, L.; Yang, H. Y.; Baumberg, J. J. Excitons in a mirror: Formation of "optical bilayers" using $MoS_2$ monolayers on gold substrates. *Appl. Phys. Lett.* **2014**, *104*, 191105.

(16) Kim, R. H.; Leem, J.; Muratore, C.; Nam, S.; Rao, R.; Jawaid, A.; Durstock, M.; McConney, M.; Drummy, L.; Rai, R.; Voevodin, A.; Glavin, N. Photonic crystallization of two-dimensional MoS2 for stretchable photodetectors. *Nanoscale* **2019**, *11*, 13260−13268.

(17) Rissner, F.; Rangger, G. M.; Hofmann, O. T.; Track, A. M.; Heimel, G.; Zojer, E. Understanding the Electronic Structure of Metal/SAM/Organic-Semiconductor Heterojunctions. *ACS Nano* **2009**, *3*, 3513−3520.

(18) Kobayashi, S.; Nishikawa, T.; Takenobu, T.; Mori, S.; Shimoda, T.; Mitani, T.; Shimotani, H.; Yoshimoto, N.; Ogawa, S.; Iwasa, Y. Control of carrier density by self-assembled monolayers in organic field-effect transistors. *Nat. Mater.* **2004**, *3*, 317−322.

(19) Liu, C.; Xu, Y.; Noh, Y.-Y. Contact engineering in organic field-effect transistors. *Mater. Today* **2015**, *18*, 79−96.

(20) Ravi, S. K.; Sun, W.; Nandakumar, D. K.; Zhang, Y.; Tan, S. C. Optical manipulation of work function contrasts on metal thin films. *Sci. Adv.* **2018**, *4*, No. eaao6050.

(21) Tseng, C.-T.; Cheng, Y.-H.; Lee, M.-C. M.; Han, C.-C.; Cheng, C.-H.; Tao, Y.-T. Study of anode work function modified by self-assembled monolayers on pentacene/fullerene organic solar cells. *Appl. Phys. Lett.* **2007**, *91*, 233510.

(22) Hedlund, J. K.; Walker, A. V. Polytype control of $MoS_2$ using chemical bath deposition. *J. Chem. Phys.* **2019**, *150*, 174701.

(23) Zhou, C.; Walker, A. V. Dependence of Patterned Binary Alkanethiolate Self-Assembled Monolayers on ″UV-Photopatterning″ Conditions and Evolution with Time, Terminal Group, and Methylene Chain Length. *Langmuir* **2006**, *22*, 11420−11425.
(24) Smith, R. K.; Lewis, P. A.; Weiss, P. S. Patterning Self-Assembled Monolayers. *Prog. Surf. Sci.* **2004**, *75*, 1−68.
(25) Fisher, G. L.; Hooper, A. E.; Opila, R. L.; Allara, D. L.; Winograd, N. The Interaction of Vapor-Deposited Al Atoms with $CO_2H$ Groups at the Surface of a Self-Assembled Alkanethiolate Monolayer on Gold. *J. Phys. Chem. B* **2000**, *104*, 3267−3273.
(26) Fisher, G. L.; Walker, A. V.; Hooper, A. E.; Tighe, T. B.; Bahnck, K. B.; Skriba, H. T.; Reinard, M. D.; Haynie, B. C.; Opila, R. L.; Winograd, N.; Allara, D. L. Bond Insertion, Complexation and Penetration Pathways of Vapor-Deposited Aluminum Atoms with HO- and $CH_3O$- Terminated Organic Monolayers. *J. Am. Chem. Soc.* **2002**, *124*, 5528−5541.
(27) Zhou, C.; Walker, A. V. Formation of Multilayer Ultrathin Assemblies Using Chemical Lithography. *Langmuir* **2010**, *26*, 8441−8449.
(28) Windom, B. C.; Sawyer, W. G.; Hahn, D. W. A Raman Spectroscopic Study of $MoS_2$ and $MoO_3$: Applications to Tribological Systems. *Tribol. Lett.* **2011**, *42*, 301−310.
(29) Jiménez Sandoval, S.; Yang, D.; Frindt, R. F.; Irwin, J. C. Raman study and lattice dynamics of single molecular layers of $MoS_2$. *Phys. Rev. B: Condens. Matter Mater. Phys.* **1991**, *44*, 3955−3962.
(30) Nayak, A. P.; Pandey, T.; Voiry, D.; Liu, J.; Moran, S. T.; Sharma, A.; Tan, C.; Chen, C.-H.; Li, L.-J.; Chhowalla, M.; Lin, J.-F.; Singh, A. K.; Akinwande, D. Pressure-Dependent Optical and Vibrational Properties of Monolayer Molybdenum Disulfide. *Nano Lett.* **2015**, *15*, 346−353.
(31) Eda, G.; Yamaguchi, H.; Voiry, D.; Fujita, T.; Chen, M.; Chhowalla, M. Photoluminescence from Chemically Exfoliated $MoS_2$. *Nano Lett.* **2011**, *11*, 5111−5116.
(32) Upon exfoliation these films were placed on Si wafers to facilitate XPS and Raman spectroscopic analyses.
(33) Jiang, Z.; Zhang, W.; Jin, L.; Yang, X.; Xu, F.; Zhu, J.; Huang, W. Direct XPS Evidence for Charge Transfer from a Reduced Rutile TiO2(110) Surface to Au Clusters. *J. Phys. Chem. C* **2007**, *111*, 12434−12439.
(34) Lee, H. J.; Jamison, A. C.; Lee, T. R. Surface Dipoles: A Growing Body of Evidence Supports Their Impact and Importance. *Acc. Chem. Res.* **2015**, *48*, 3007−3015.
(35) Alloway, D. M.; Hofmann, M.; Smith, D. L.; Gruhn, N. E.; Graham, A. L.; Colorado, R.; Wysocki, V. H.; Lee, T. R.; Lee, P. A.; Armstrong, N. R. Interface Dipoles Arising from Self-Assembled Monolayers on Gold: UV−Photoemission Studies of Alkanethiols and Partially Fluorinated Alkanethiols. *J. Phys. Chem. B* **2003**, *107*, 11690−11699.
(36) Lee, S.-H.; Lin, W.-C.; Chang, C.-J.; Huang, C.-C.; Liu, C.-P.; Kuo, C.-H.; Chang, H.-Y.; You, Y.-W.; Kao, W.-L.; Yen, G.-J.; Kuo, D.-Y.; Kuo, Y.-T.; Tsai, M.-H.; Shyue, J.-J. Effect of the chemical composition on the work function of gold substrates modified by binary self-assembled monolayers. *Phys. Chem. Chem. Phys.* **2011**, *13*, 4335−4339.
(37) Lim, H. S.; Lee, W. H.; Lee, S. G.; Lee, D.; Jeon, S.; Cho, K. Effect of nanostructure on the surface dipole moment of photo-reversibly tunable superhydrophobic surfaces. *Chem. Commun.* **2010**, *46*, 4336−4338.


https://dx.doi.org/10.1021/acs.langmuir.9b01964
*Langmuir* 2020, 36, 682−688